Supporting Information for

Synthesis of Small Ag-Sb-Te Nanocrystals with Composition Control

Annina Moser, Olesya Yarema, Maksym Yarema and Vanessa Wood*

Department of Information Technology and Electrical Engineering, ETH Zurich, Gloriastrasse 35, CH-8092 Zurich, Switzerland

*E-mail: vwood@ethz.ch.

Figures S1 and S2 show high-resolution transmission electron microscope (HR-TEM) images of $AgSbTe_2$ particles and selected area electron diffraction (SAED) from the specific regions of the HR-TEM image. These images highlight that the nanocrystals are single crystalline and have a cubic crystal structure.

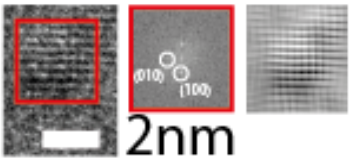

Fig. S1: HR-TEM image showing a particle with lattice fringes of 0.304 nm spacing in two directions perpendicular to each other, which correspond to the (100) and (010) planes of cubic $AgSbTe_2$. SAED image is given in the middle. A reconstructed image from filtered FFT is displayed on the right.

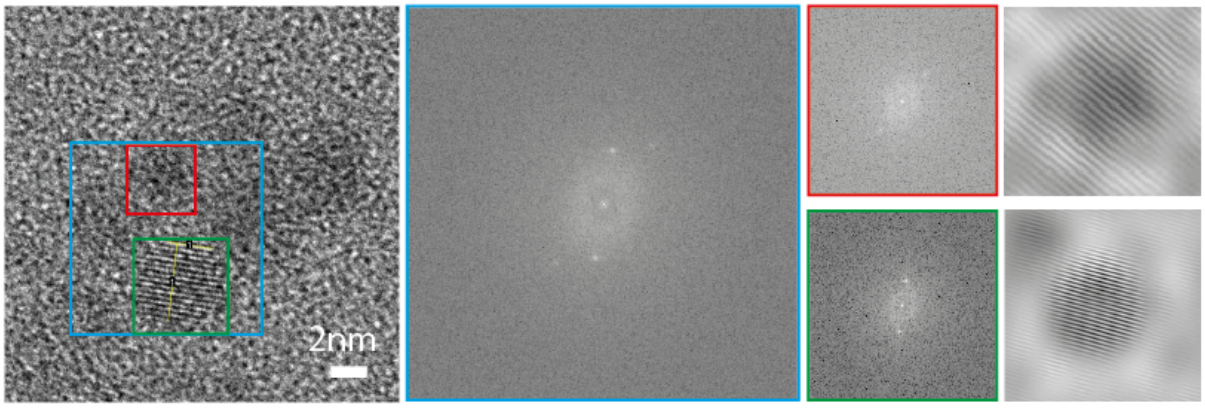

Fig. S2: The upper particle (red, solid) shows faint lattice fringes with a spacing of 0.21 nm (determined via SAED). The lower particle (yellow, dashed) shows distinct lattice fringes with 0.303 nm spacing. These correspond to the (110) and (100) planes of $AgSbTe_2$, respectively. SAED images are given in the middle, reconstructed images from filtered FFT on the right.

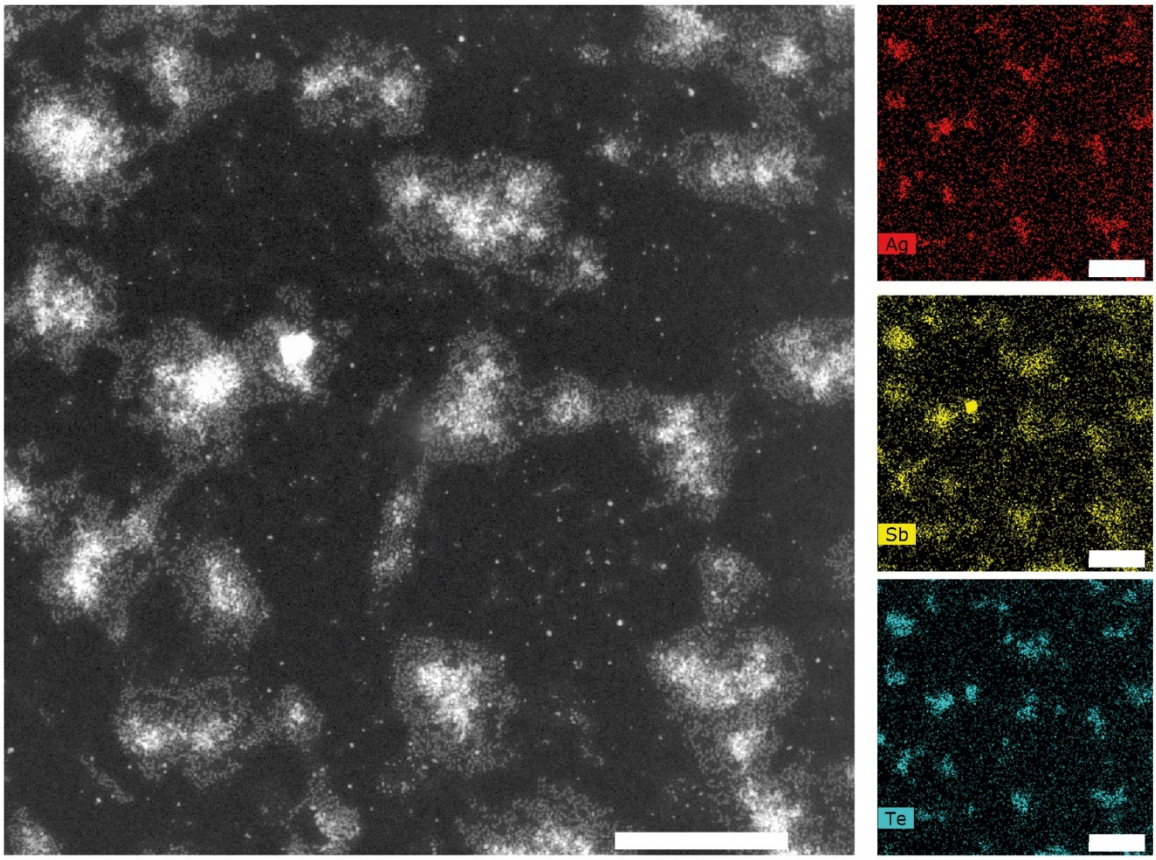

Fig. S3: STEM-image of stoichiometric $AgSbTe_2$ and elemental maps from STEM/EDX for Ag, Sb and Te. The presence of all elements across the region indicate that nanocrystals are ternary. All scale bars correspond to 200nm.

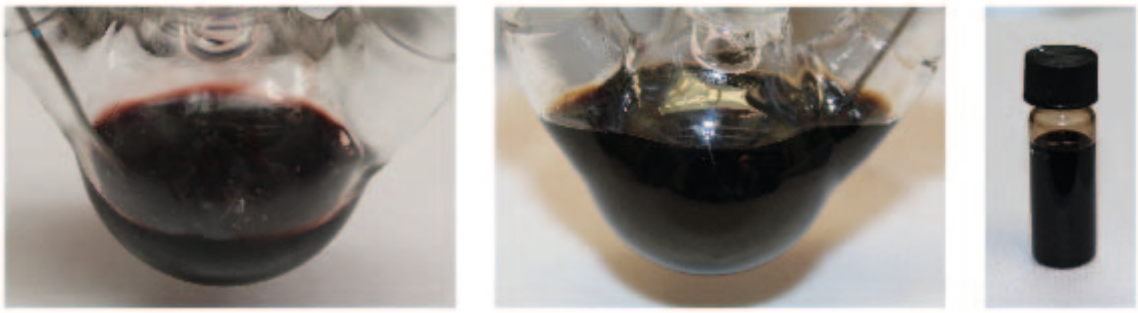

Fig. S4: Photographs of the synthesis after 1h (left), after adding oleic acid (middle), and after washing (right). The dark purple color stems from polytellurides that form because of the large excess of anion precursor in TOP and oleylamine. As soon as oleic acid is added to the system, oleic acetate and oleyl-ammonium ions form. Ammonium ions can easily capture Te-ions, which causes the breaking of polytelluride bonds and therefore change of color to brown.

Table S1: Elemental compositions of Ag-Sb-Te compounds compared to cation precursor ratio measured with EDX. Errors are given in brackets.

at% Ag precursor	*at% Sb precursor*	*at% Ag*	*at% Sb*	*at% Te*
70	30	55(2)	6(12)	39(4)
65	35	49(2)	8(9)	43(4)
60	40	32(2)	18(5)	50(4)
55	45	25(3)	22(4)	53(3)
50	50	23(3)	23(4)	54(3)
45	55	21(3)	26(3)	53(3)
40	60	19(1)	29(1)	52(1)
35	65	16(4)	29(3)	55(2)
30	70	13(4)	31(3)	56(2)
25	75	9(5)	33(2)	58(2)
20	80	8(5)	33(2)	60(2)

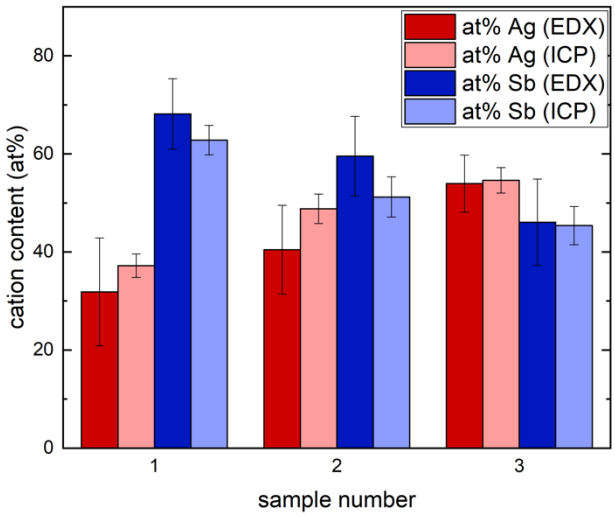

Fig. S5: Comparison of elemental analyses with EDX and ICP-OES. For the ICP-OES measurement, two portions of about 8 mg each from the same Ag-Sb-Te sample were dried under vacuum and weighed. One portion was diluted in concentrated HNO_3 in order to measure the Ag content the other portion was diluted in concentrated H_2SO_4 in order to measure the Sb content, and both were dissolved for >24h. The samples were then diluted to a 5% acid solution and 5-15 ppm cation content. Each sample was measured five times on an Agilent 720S, and the tubes were flushed for at least 45 s with clean matrix acid between sample measurements. Results were compared to a multi-element ICP Calibration Standard from CPAChem. Lithium peaks were consistently within the background level of the blank reference. Since Ag and Sb content were measured from different sample portions (dissolved in HNO_3 and H_2SO_4, respectively), deviations due to weighing and titration, as well as the use of two different matrix acids, limit the precision. Errors from weighing, titration, and measurement variation are included in the error bars. A good agreement between the EDX analysis and the ICP-OES measurements is found.

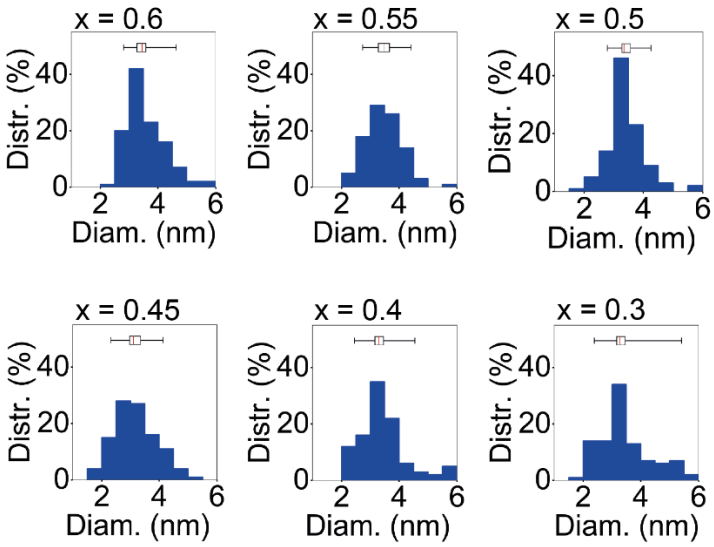

Fig. S6: Histograms of single-phase compositions of $Ag_xSb_{1-x}Te_{1.5-x}$. The red line corresponds to the median, the box to the true median interval and the whiskers to the $P_{15.87} = P_{-1Z}$ and $P_{84.13} = P_{+1Z}$ percentiles with a 95% confidence interval[1]. The median size stays approximately constant, while the $P_{84.13}$ values go to larger sizes for very Ag- and Sb-rich compositions. The further away in composition one is from $AgSbTe_2$, for which the synthesis was optimized, the more likely agglomerates are formed.

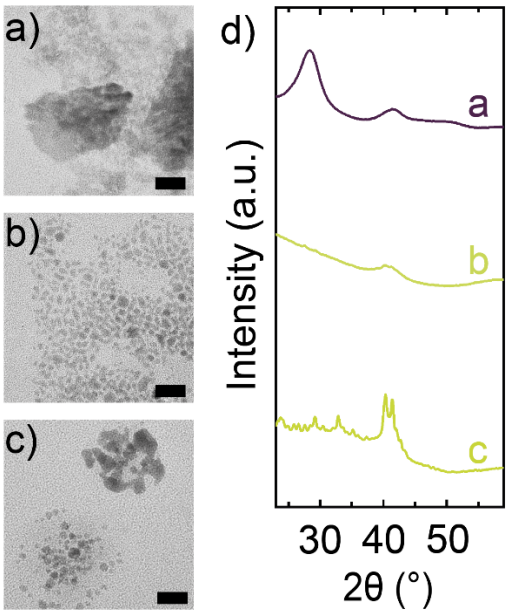

Fig. S7: TEM images of Ag-Sb-Te composition series with a Ag:Sb cation precursor ratio of 2:8 (a), 6.5:3.5 (b) and 7:3 (c) and corresponding XRD patterns. For precursor ratios of Ag:Sb smaller than 3:7, platelets are formed as a second phase. While Sb_2Te_3 diffraction peaks cannot be identified in XRD, TEM shows clear Sb_2Te_3 platelet structures as an admixture to the ternary $Ag_xSb_{1-x}Te_{1.5-x}$ nanocrystals. If the Ag:Sb precursor ratio is greater than 6:4, the final product contains large accumulations of nanoparticles with no antimony. The precursor ratio of 6.5:3.5 leads to a product with no clear XRD pattern, suggesting the product to be amorphous. The precursor ratio of 7:3 exhibits sharp diffraction peaks, which cannot be assigned to a particular Ag-Te compound.

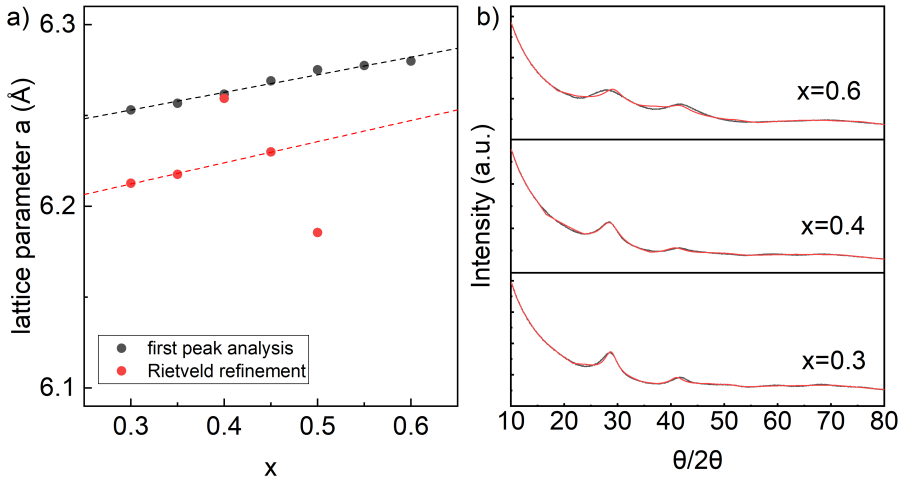

Fig. S8: (a) Lattice constants derived from the analysis of the first peak (black) as well as from Rietveld refinement (red) and (b) representative fits for the $Ag_xSb_{1-x}Te_{1.5-x}$ nanocrystals with different composition, x. Due to broad features stemming from the nanocrystal size, Rietveld refinement was performed using a limited amount of parameters, which decreases the reliability of results. The cubic structure, Fm-3m, was used with fixed occupancies corresponding to the measured elemental composition. Scale, background, overall thermal factor, size-dependent broadening and the lattice parameter were refined, and results are tabulated below. For $x < 0.5$, the trend of increasing lattice constant with increasing Ag-content is observed. For $x \geq 0.5$, no good fit can be achieved (e.g., see upper panel of b for x=0.6) and the resulting refined lattice constants cannot be considered accurate. It is likely that more complex structures featuring ordered cations are present for larger x content.

Table S2: Rietveld refinement fitted parameters for $Ag_xSb_{1-x}Te_{1.5-x}$ with varying x.

x	***lattice parameter***	***Thermal factor***	***Peak broadening***	***Bragg R factor***	***Bragg Rf factor***
0.6	6.12	7.6	14.9	9.01	7.92
0.55	6.10	11.4	16.1	8.15	7.96
0.5	6.19	17.6	14.1	6.79	11.6
0.45	6.23	11.3	14.2	2.42	2.94
0.4	6.26	19.3	16.9	3.05	5.69
0.35	6.22	14.1	7.0	4.59	5.15
0.3	6.21	15.8	6.5	5.04	5.91

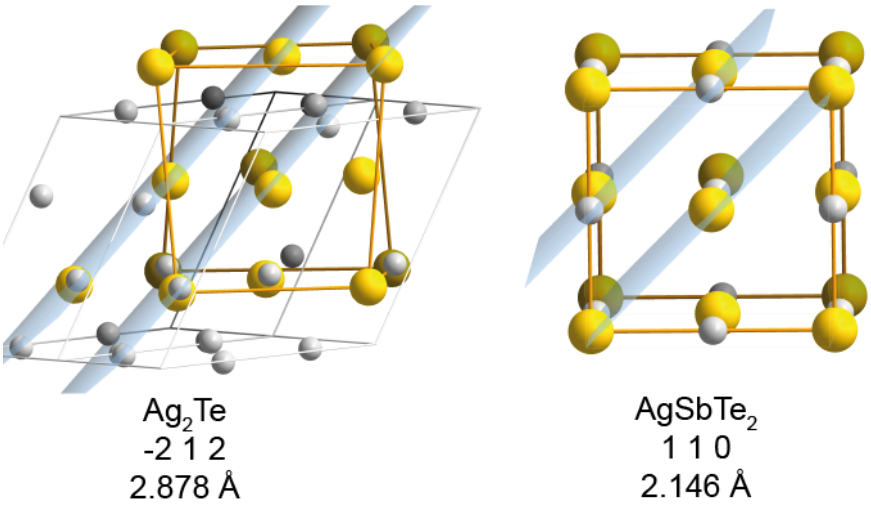

Fig. S9: Selected planes and interplanar distances of major diffraction peaks of Ag_2Te and $AgSbTe_2$. The spacing of Tellurium atoms is significantly larger in the binary crystal.

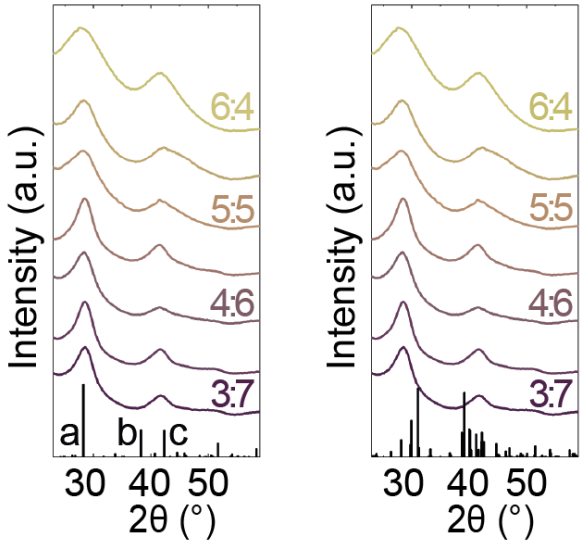

Fig. S10: Measured XRD pattern of the NCs with Sb_2Te_3 (left) and Ag_2Te (right) reference peaks, respectively. The second major diffraction peak of Sb_2Te_3 (b) is situated in the valley or at the very beginning of the second measured broad peak. Similarly, the measured patterns do not match the two assemblies of peaks of Ag_2Te.

References to the Supporting Information

(1) Schmid, H.; Huber, A. The 3σ Fallacy. IEEE Microw. Mag. 2014, 15 (7), 68–74. https://doi.org/10.1109/MMM.2014.2355954.